Reflection and transmission of Laguerre-Gaussian beams in a dielectric slab

Haiying Li, Farideh Honary, Zhensen Wu, Lu Bai

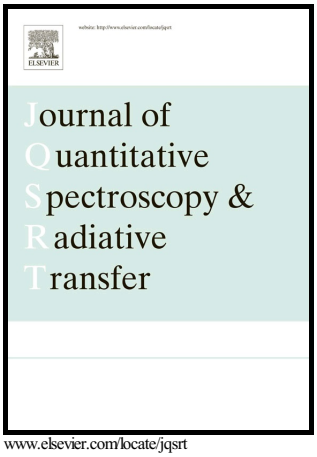

www.elsevier.com/locate/jqsrt

PII: S0022-4073(16)30508-8
DOI: http://dx.doi.org/10.1016/j.jqsrt.2016.12.001
Reference: JQSRT5515

To appear in: *Journal of Quantitative Spectroscopy and Radiative Transfer*

Received date: 26 August 2016
Revised date: 28 November 2016
Accepted date: 1 December 2016

Cite this article as: Haiying Li, Farideh Honary, Zhensen Wu and Lu Bai Reflection and transmission of Laguerre-Gaussian beams in a dielectric slab *Journal of Quantitative Spectroscopy and Radiative Transfer*, http://dx.doi.org/10.1016/j.jqsrt.2016.12.001

REFLECTION AND TRANSMISSION OF LAGUERRE-GAUSSIAN BEAMS IN A DIELECTRIC SLAB

Haiying Li[a,b,c*], Farideh Honary[c], Zhensen Wu[a,b] and Lu Bai[a,b]

[a]School of Physics and Optoelectronic Engineering, Xidian University, Xi'an, 710071, China

[b]Collaborative Innovation Center of Information Sensing and Understanding at Xidian University, Xi'an, 710071, China

[c]Department of Physics, Lancaster University, Lancaster, UK

[*]*Corresponding author: lihy@xidian.edu.cn*

Abstract

This paper considers the reflection and transmission characteristics of a Laguerre-Gaussian (LG) beam in a dielectric slab. The fields of the reflected and transmitted beams are described based on plane-wave angular spectrum representation. Using the generalized Fresnel amplitude reflectance and transmittance, the reflected and transmitted fields in each region are expressed. With the Taylor series approximation of reflectance and transmittance, the analytical expressions of the total reflected and transmitted fields in the input and output regions are derived. The effects of the beam-waist radius and topological charge on the reflected and transmitted field intensities are simulated and discussed in detail. The centroid shifts of the reflected beam are also presented. It is concluded that the distortion of the intensity distribution including the size of the intensity contour, is influenced by the beam-waist radius and the topological charge of the incident beam. The total intensity of the slab, in particular for the case of the transmitted field, is found to be distinguishable from the case of the single interface.

Keywords

Reflection and transmission, Laguerre Gaussian beam, Dielectric slab

1. Introduction

Since the Laguerre-Gaussian (LG) beam was demonstrated to possess orbital angular momentum(OAM) [1], the generation methods, propagation characteristics and application of electromagnetic beams with OAM [2-5] have been attracting the attention of many scholars and have been widely used in the fields of optical manipulation [6], quantum and optical information [7,8], optical detection [9], and object recognition[10].

The interaction of electromagnetic beams with different media [11-18] is an important topic that has been extensively studied in the past several decades. As early as the 1970s, the reflection and transmission of Gaussian beams in a dielectric interface have been developed by several methods [19-21]. For the vortex beams incident on a

dielectric interface, Bliokh predicted a novel vortex-induced Goos- Hänchen (GH) shift in the reflected and transmitted fields of polarized vortex beams [22, 23]. Petrov discussed the reflectance of a strongly focused vector beams at normal incidence [24]. Okuda discussed the deformations of reflected and transmitted fields from a dielectric interface as the LG beam was incident near critical angle, and compared the experimental and theoretical results [25]. With the full Taylor series expansion, the reflection of LG beams in a dielectric interface was presented by Ou [26], which held in both the paraxial and nonparaxial regimes. Therefore, profound research results have been achieved on the reflection and transmission of beams from a dielectric interface, not only in terms of the GH and Imbert-Fedorov (IF) shifts but also the intensity deformation properties. Generally, the angular spectrum method is one of the important methods to determine the reflection and transmission of beams. In these studies, Snell's law, the Fresnel coefficients and the generalized Fresnel amplitude reflectance and transmittance of a plane wave are used.

Regarding applications involving the propagation of beams, it is important to understand the effects that various media have on beams (such as Gaussian beams and LG beams). The reflection and transmission of a plane wave in media can be analyzed using the well-known Snell's law and Fresnel formulas. However, for the propagation of beams with a finite width in media, the problem becomes complex. Riesz investigated three factors that affect the path of the peak of the reflected profile of a Gaussian beam from a dielectric slab [27]. The propagation of continuous wave (CW) Gaussian beams in a double negative metamaterial slab [28] was simulated using a two-dimensional finite-difference time-domain(FDTD) approach. Based on the Generalized Lorenz-Mie theory (GLMT) framework, the reflection and transmission of a Gaussian beam from a uniaxial anisotropic slab [29] were solved by using Vector Cylindrical Wave Functions (VCWFs) expansion of beams and boundary conditions of electromagnetic fields. Kong [30] studied the unique negative lateral shift of a Gaussian beam in the double negative slab. Galiatsatos [31] simulated the transmittance of a plane wave in a dielectric slab and discussed the electromagnetic force exerted on a dielectric sphere that was placed in the slab. For the inhomogeneous media, much work has been developed to investigate the propagation of beams in inhomogeneous media [32-36], such as the GH shifts of reflected beams for the inhomogeneous slab [32], the nonspecular phenomena of the reflected fields [33], the absorption and lateral shift of the beams in the lossy multilayered media [34], and the ultrasound beam propagation in inhomogeneous tissue geometries [35]. Although the reflection and transmission of a Gaussian beam in a slab have been studied by several different methods, the propagation characteristics of an LG beam in a dielectric slab has not been reported; reporting these characteristics is the purpose of this work.

In this paper, the reflection and transmission of LG beams in a dielectric slab are presented based on the angular spectrum expansion and the generalized Fresnel amplitude reflectance and transmittance of the plane waves. The reflected and transmitted fields in each region for LG beams incidence are expressed by the angular spectrum in Section 2.1. Considering an isotropic homogeneous dielectric slab, the analytical expressions of the reflected and transmitted fields are derived in Section 2.2. The numerical results of the reflected and transmitted field intensities for lossless and lossy slabs are provided, and a discussion of the effects of the beam-waist radius, the topological charge and the centroid shifts of the reflected beam is also given in Section 3. Finally, Section 4 presents a summary of the conclusion of our work.

2. Theoretical Backgrounds

We consider the reflection and transmission of an LG beam in a dielectric slab, which is shown in Figure 1. In the global coordinate (x, y, z) of this system, the $x-y$ plane is situated on the first interface ($z=0$), and the principal plane of incidence is the $x-z$ plane. The coordinate values z corresponding to each interface are z_0, z_1. The input and output planes are infinite half spaces, and the thickness of the slab is d_1. We are concerned with the LG beam incident upon the slab at an angle ϕ_i measured with respect to the z axis in the $x-z$ plane. The reflection and transmission directions are described by the angles $\phi_r = \pi - \phi_i$ and ϕ_t. The refractive index, dielectric constant and wave number of each region are n_j ε_j and k_j, respectively. The magnetic susceptibility of each region is assumed to be unity. The $x_\alpha - y_\alpha$ planes in the local coordinates $(x_\alpha, y_\alpha, z_\alpha)$ $\alpha = i, r \text{ or } t$ define the transverse planes of the incident, reflected and transmitted beams, and the z_α axis is coincident with the geometric-optical axis of the corresponding beam.

Supposing the origin of the coordinates (x_i, y_i, z_i) and (x_r, y_r, z_r) are located at $(x=0, y=0, z=0)$, then the transformations between the coordinates (x_i, y_i, z_i) , (x_r, y_r, z_r) and the global coordinates are $x = x_{i,r}\cos\phi_{i,r} + z_{i,r}\sin\phi_{i,r}$, $y = y_{i,r}$ and $z = -x_{i,r}\sin\phi_{i,r} + z_{i,r}\cos\phi_{i,r}$, respectively. The origin of the coordinates (x_t, y_t, z_t) is located at $(x = x_0, y = 0, z = z_0)$; thus, we can obtain $x = x_0 + x_t\cos\phi_t + z_t\sin\phi_t$, $y = y_t$ and $z = z_0 - x_t\sin\phi_t + z_t\cos\phi_t$.

Meanwhile, the relationship between the wave number components (k_x, k_y, k_z) and (k_{ix}, k_{iy}, k_{iz}) is given by $k_x = k_{ix}\cos\phi_i + \sqrt{k_i^2 - k_{ix}^2 - k_{iy}^2}\sin\phi_i$, $k_y = k_{iy}$ and $k_z = -k_{ix}\sin\phi_i + \sqrt{k_i^2 - k_{ix}^2 - k_{iy}^2}\cos\phi_i$.

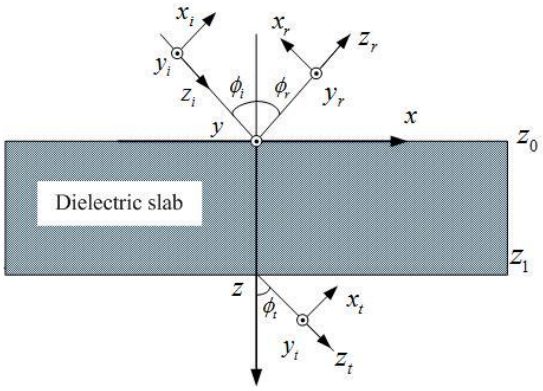

Figure1 *Coordinate system definition for the reflection and transmission of an LG beam incident on a dielectric slab.*

2.1 Electric field expressions of an LG beam incident on a dielectric slab based on the plane-wave angular spectrum

Assuming that a linearly polarized LG beam is incident on a dielectric slab, when the focal plane of the incident beam is at $z_i = 0$, the complex electric field amplitude of the LG beam in the incident plane can be written as:

$$E_i(r_i, \theta_i, z_i = 0) = E_0\left[\frac{\sqrt{2}r_i}{w_0}\right]^{|l|}\exp\left[\frac{-r_i^2}{w_0^2}\right]L_p^{|l|}\left(\frac{2r_i^2}{w_0^2}\right)\exp(-il\theta_i) \tag{1}$$

In equation (1), the cylindrical coordinate system is chosen, and the relationship between (r_i, θ_i, z_i) and (x_i, y_i, z_i) is $r_i = \sqrt{x_i^2 + y_i^2}$ and $\theta_i = \text{atan}(y_i / x_i)$. The factor $E_0 = \sqrt{2p!/\pi(p+|l|)!}/w_0$ is the amplitude constant, w_0 is the beam-waist radius, and $L_p^{|l|}(\cdot)$ is the associated Laguerre polynomial. p and l represent the LG mode radial index and the topological charge, respectively. The time dependence of $\exp(-i\omega t)$ is omitted.

Using the two-dimension Fourier transform, the angular spectrum amplitude of the incident LG beam [26] in its focal plane can be written as:

$$\begin{aligned}\overline{E}_i(k_i, \varphi_i) &= \frac{1}{2\pi}\int_0^\infty\int_0^{2\pi} E_i(r_i, \theta_i, z_i = 0)\exp\left[-ik_i r_i\cos(\theta_i - \varphi_i)\right] r_i dr_i d\theta_i \\ &= E_0 i^l(-1)^{p+1}\exp(-il\varphi_i)\left(\frac{w_0}{\sqrt{2}}\right)^2\left(\frac{k_i}{\sqrt{2}k_0 f}\right)^l\cdot\exp\left(-\frac{k_i^2}{4k_0^2 f^2}\right)L_p^{|l|}\left(\frac{k_i^2}{2k_0^2 f^2}\right)\end{aligned} \tag{2}$$

where k_i is the wave number in the incident space, and $f = 1/k_0 w_0$ is the natural expansion factor [37]. The

coordinates (k_i, φ_i) represent the spectrum space.

Snell's law, the Fresnel coefficients or the generalized Fresnel amplitude reflectance and transmittance can be applied to the plane wave angular spectrum elements of the beam directly. The electric field components can then be derived utilizing the integral of inverse Fourier transform from the angular spectrum of beam amplitude.

The angular spectrum of incident and reflected waves above the first interface can be expressed as:

$$\overline{E}_i(k_i, \varphi_i) \exp(ik_{i,z} z_i) \quad , r_{0,1}^2 \overline{E}_i(k_i \ \varphi_i), \quad \exp(ik_{r,z} z_r) \tag{3}$$

where $r_{0,1}^2$ takes into account not only the reflection from the first interface, but also multiple reflections and transmissions from all deeper interfaces.

In the internal region of the dielectric slab, the angular spectrum has the following forms:

$$\overline{E}_1(k_1, \varphi_1, z_1) = \overline{E}_1^i(k_1^i, \varphi_1^i) \exp(ik_{1,z}^i z_1^i) \hat{k}_1^i + r_{1,2}^1 \overline{E}_1^i(k_1^i, \varphi_1^i) \exp(ik_{1,z}^r z_1^r) \hat{k}_1^r \tag{4}$$

where the first term represents the angular spectrum of the downward-going component, which includes the transmitted element from the first interface and all the reflected elements between the two interfaces, and the second term denotes all the reflected components from the second interface.

In the transmitted region, there is only a transmitted wave and no reflected wave; therefore:

$$\overline{E}_{N+1}^t(k_t, \varphi_t, z_t) = t_{0,2}^2 \cdot \overline{E}_i(k_i, \varphi_i) \exp(ik_{t,z} z_t) \tag{5}$$

where $t_{0,2}^2$ is the total amplitude transmittance. Making use of the generalized Fresnel amplitude reflectance and transmittance of plane wave in inhomogeneous media, the total angular spectrum in the slab is derived to be:

$$\overline{E}_1(k_1, \varphi_1, z_1) == \frac{\overline{E}_1^i(k_1^i, \varphi_1^i)}{\overline{E}_i(k_i, \varphi_i)} \left[\hat{k}_1^i + r_{1,2}^1 \exp(ik_{1,z}^r z_1^r - ik_{1,z}^i z_1^i) \hat{k}_1^r \right] \overline{E}_i(k_i, \varphi_i) \exp(ik_{1,z}^i z_1^i) \tag{6}$$

where $\overline{E}_1^i(k_1^i, \varphi_1^i) / \overline{E}_i(k_i, \varphi_i) = \left[t_{0,1}^1 \exp(-ik_{i,z} z_i) \exp(-ik_{1,z}^i z_0') \right] / \left[1 - r_{1,0}^1 r_{1,2}^1 \exp(i2k_{1,z}^i d_1') \right]$, and $d_1' = z_1' - z_0'$. In equations (4)-(6), the local coordinates $(x_1^\beta, y_1^\beta, z_1^\beta)$ $\beta = i, r$, which are located at the second interface, are used to describe the incident and reflected beams in the slab. In the internal region of the slab, the positive direction of z_1^β axis coincides with the geometric-optical axis of the corresponding beams. The unit vectors $\hat{k}_1^i$ and $\hat{k}_1^r$ point to the positive directions of z_1^i and z_1^r axes, respectively. z_0' and z_1' are the coordinate values of the first and second interfaces in the incident coordinates, respectively.

With the inverse Fourier transformation of the expressions above, the corresponding complex electric field amplitude

in the dielectric slab can be derived as:

$$E\left(r_1,\theta_1,z_1\right)=\frac{1}{2\pi}\int_0^{\infty}\int_0^{2\pi}\overline{E}_1\left(k_1,\varphi_1,z_1\right)\exp\left[ik_1r_1\cos\left(\theta_1-\varphi_1\right)\right]k_1dk_1d\varphi_1 \tag{7}$$

Meanwhile, the reflected electric field in the local coordinate (x_r,y_r,z_r) above the first interface is:

$$E_r\left(r_r,\theta_r,z_r\right)=\frac{1}{2\pi}\int_0^{\infty}\int_0^{2\pi}r_{0,1}^2\overline{E}_i\left(k_i,\varphi_i\right)\exp(ik_{r,z}z_r)\exp\left[ik_rr_r\cos\left(\theta_r-\varphi_r\right)\right]k_rdk_rd\varphi_r \tag{8}$$

The transmitted electric field (x_t,y_t,z_t) in the output region is:

$$E_t\left(r_t,\theta_t,z_t\right)=\frac{1}{2\pi}\int_0^{\infty}\int_0^{2\pi}t_{0,2}^2\cdot\overline{E}_i\left(k_i,\varphi_i\right)\exp(ik_{t,z}z_t)\exp\left[ik_tr_t\cos\left(\theta_t-\varphi_t\right)\right]k_tdk_td\varphi_t \tag{9}$$

According to the boundary condition of electromagnetic fields, the generalized amplitude reflectance [38] for an N-layers media can be expressed with a recursive form, that is:

$$r_{j,j+1}^{N-j}=\frac{r_{j,j+1}^1+r_{j+1,j+2}^{N-j-1}\exp(i2k_{j+1,z}d_{j+1})}{1+r_{j,j+1}^1r_{j+1,j+2}^{N-j-1}\exp(i2k_{j+1,z}d_{j+1})},\ \text{where: } r_{N,N+1}=0 \tag{10}$$

The total amplitude transmittance is:

$$t_{0,N}^N=\prod_{j=0}^{N}\exp(ik_{j,z}d_j)S_{j,j+1} \tag{11}$$

where $S_{j,j+1}=t_{j,j+1}^1\Big/\left[1-r_{j+1,j}^1r_{j+1,j+2}^{N-j-1}\exp(i2k_{j+1,z}d_{j+1})\right]$.

The $r_{j,j+1}^1$ and $t_{j,j+1}^1$ in equations (10) and (11) are the Fresnel reflection and transmission coefficients, respectively. For the parallel and vertical polarizations, they are given by[38]:

$$\begin{aligned}r_{j,j+1}^{1,p}&=\frac{n_{(j+1),j}^2k_{j,z}-k_{j+1,z}}{n_{(j+1),j}^2k_{j,z}+k_{j+1,z}} \qquad p-polarization(Parallel\ \ polarization)\\ r_{j,j+1}^{1,s}&=\frac{k_{j,z}-k_{j+1,z}}{k_{j,z}+k_{j+1,z}} \qquad s-polarization(Vertical\ \ polarization)\end{aligned} \tag{12}$$

$$\begin{aligned}t_{j,j+1}^{1,p}&=\frac{\cos\phi_j}{\cos\phi_{j+1}}\left[1-r_{j,j+1}^{1,p}\right] \qquad p-polarization(Parallel\ \ polarization)\\ t_{j,j+1}^{1,s}&=1+r_{j,j+1}^{1,s} \qquad s-polarization(Vertical\ \ polarization)\end{aligned} \tag{13}$$

where $k_{j,z}=\sqrt{k_j^2-k_{j,x}{}^2-k_{j,y}{}^2}$ and $k_{j+1,z}=\sqrt{k_{j+1}^2-k_{j+1,x}{}^2-k_{j+1,y}{}^2}$ represent the longitudinal components of the wave vectors in the j^{th} and $(j+1)^{\text{th}}$ layers, respectively. ϕ_j and ϕ_{j+1} are the incident angles of the j^{th} and

$(j+1)^{\text{th}}$ interfaces, respectively. The *p*-polarization represents the direction of the incident electric field is parallel to the x_i axis, whereas the *s*-polarization denotes the incident electric field which is parallel to the y_i axis.

2.2 Approximate expressions of reflected and transmitted fields from a homogeneous dielectric slab

Considering an *s*-polarized LG beam that is incident on a dielectric slab from a homogeneous media space and then leaves the slab into the other homogeneous media. The equation (8) shows the total reflected field. $r_{0,1}^2$ is the total generalized amplitude reflectance and can be expanded as the following expression (here, to reduce calculation, we retain the first two terms):

$$\begin{aligned} r_{0,1}^2 &= r_{0,1}^1 + \frac{t_{0,1}^1 r_{1,2}^1 t_{1,0}^1 \exp(i2k_{1z}d_1)}{1-r_{1,0}^1 r_{1,2}^1 \exp(i2k_{1z}d_1)} \\ &\approx r_{0,1}^1 + t_{0,1}^1 r_{1,2}^1 t_{1,0}^1 \exp(i2k_{1z}d_1) \\ &= r' + r'' \end{aligned} \tag{14}$$

Noticing $r_{1,0}^1 = -r_{0,1}^1$, we have $t_{,10}^1 = 1 + r_{1,0}^1 = 1 - r_{0,1}^1$. d_1 denotes the thickness of the slab. Using the Taylor series, considering the paraxial approximation [25], the Fresnel reflection coefficients $r_{0,1}^1$ and $r_{1,2}^1$ are expanded around the center angular component of the incident beam and only retained the zero and the first terms, that is, $r_{0,1}^1 \approx r_{0,1}^1(k_{\perp 0x}) + r_{0,1}^1(k_{\perp 0x})\left(k_{\perp 0} - k_{\perp 0x}\right)Q_{r0}$, $r_{1,2}^1 \approx r_{1,2}^1(k_{\perp 1x}) + r_{1,2}^1(k_{\perp 1x})\left(k_{\perp 1} - k_{\perp 1x}\right)Q_{r1}$. The corresponding expansion of $t_{0,1}^1$ and $t_{1,0}^1$ can also be obtained conveniently.

Therefore, substituting $r_{0,1}^1$ and $r_{1,2}^1$ into equation (14), r' and r'' can be written as

$$r' = r_{0,1}^1(k_{\perp 0x}) + r_{1,2}^1(k_{\perp 1x})\left[1 - \left(r_{0,1}^1(k_{\perp 0x})\right)^2\right]\exp(i2k_{1z}d_1) \tag{15}$$

$$\begin{aligned} r'' = {} & r_{0,1}^1(k_{\perp 0x})\left(k_{\perp 0} - k_{\perp 0x}\right)Q_{r0} + \\ & \left[\left(k_{\perp 1} - k_{\perp 1x}\right)Q_{r1} - 2\left(k_{\perp 0} - k_{\perp 0x}\right)\left[r_{0,1}^1(k_{\perp 0x})\right]^2 Q_{r0}\right] r_{1,2}^1(k_{\perp 1x})\exp(i2k_{1z}d_1) \end{aligned} \tag{16}$$

where $Q_{r0} = \partial \ln r_{0,1}^1(k_{\perp 0}) / \partial k_{\perp 0}\big|_{k_{\perp 0x}}$, $Q_{r1} = \partial \ln r_{1,2}^1(k_{\perp 1}) / \partial k_{\perp 1}\big|_{k_{\perp 1x}}$. The symbol $\perp$ in subscripts represents the perpendicular component.

Substituting equations (15) and (16) into (8), the approximate analytical expression of reflected field can be obtained as

$$
\begin{aligned}
&E_r\left(r_r,\theta_r,z_r\right)=(-1)^p\exp(ik_rz_r)\Psi_{p,l}(r_r,z_r)\exp\left(il\theta_r\right)\cdot\\
&\left[r_{0,1}^1(k_{\perp 0x})\left(1-k_{\perp 0x}Q_{r0}\right)+r_{1,2}^1(k_{\perp 1x})\left(\left(1-k_{\perp 1x}Q_{r1}\right)-\left(r_{0,1}^1(k_{\perp 0x})\right)^2\left(1-2k_{\perp 0x}Q_{r0}\right)\right)\exp(i2k_1\cos\phi_1d_1)\right]\\
&+(-1)^p\exp(ik_rz_r)\exp\left(il\theta_r\right)\left[r_{0,1}^1(k_{\perp 0x})Q_{r0}+r_{12}^1(k_{\perp 1x})\left(Q_{r1}\frac{\cos\phi_1}{\cos\phi_0}-2\left(r_{0,1}^1(k_{\perp 0x})\right)^2Q_{r0}\right)\exp(i2k_1\cos\phi_1d_1)\right]\\
&\cdot\left\{\left(l\frac{\sin\theta_r}{r_r}-\frac{k_0r_0\cos\theta_r}{R\left(z_r\right)}\right)\Psi_{p,l}(r_r,z_r)+i\cos\theta_r\left[\left(\frac{|l|}{r_r}+\frac{2r_r}{w^2(z_0)}\right)\Psi_{p,l}\left(r_r,z_r\right)-\frac{2\sqrt{2}}{w(z_r)}\sqrt{p+|l|+1}\Psi_{p,l+1}\left(r_r,z_r\right)\right]\right\}
\end{aligned}
\tag{17}
$$

where $\Psi_{m,n}(r_r,z_r)=\sqrt{2m!/\pi(m+|n|)!}\left[\sqrt{2}r_r/w(z_r)\right]^{|n|}\exp\left[-r_r^{\,2}/w^2(z_r)\right]L_m^{|n|}\left(2r_r^{\,2}/w^2(z_r)\right)$. The total amplitude transmittance is as follows:

$$
\begin{aligned}
t_{0,2}^2&=\frac{t_{0,1}^1t_{1,2}^1\exp(ik_{1,z}d_1)}{1-r_{1,0}^1r_{1,2}^1\exp(i2k_{1,z}d_1)}\\
&\approx t_{0,1}^1t_{1,2}^1\exp(ik_{1,z}d_1)+t_{0,1}^1r_{1,0}^1r_{1,2}^1t_{1,2}^1\exp(i3k_{1,z}d_1)\\
&=t'+t''
\end{aligned}
\tag{18}
$$

Using a similar process as that of the total generalized amplitude reflectance, the two parts t' and t'' are presented by:

$$
t'=t_{0,1}^1\left(k_{\perp 0x}\right)t_{1,2}^1\left(k_{\perp 1x}\right)\exp(ik_{1,z}d_1)\left[1-r_{0,1}^1\left(k_{\perp 0x}\right)r_{1,2}^1\left(k_{\perp 1x}\right)\exp(i2k_{1,z}d_1)\right]
\tag{19}
$$

$$
\begin{aligned}
t''=&t_{0,1}^1\left(k_{\perp 0x}\right)t_{1,2}^1\left(k_{\perp 1x}\right)\exp(\mathrm{i}k_{1,z}d)\left\{\left[\left(k_{\perp 2x}\eta_2Q_{t1}+k_{\perp 1x}\eta_1Q_{t0}+k_{\perp 2x}\eta_2k_{\perp 1x}\eta Q_{t0}Q_{t1}\right)\right]-\right.\\
&\left.r_{0,1}^1\left(k_{\perp 0x}\right)r_{1,2}^1\left(k_{\perp 1x}\right)\left[\left(k_{\perp 2x}\eta_2Q_{t1}+k_{\perp 1x}\eta_1Q_{t0}\right)+\left(k_{\perp 1}Q_{r1}-k_{\perp 0}Q_{r0}\right)\right]\exp(\mathrm{i}2k_{1,z}d)\right\}
\end{aligned}
\tag{20}
$$

where $\eta_1=\cos\phi_1/\cos\phi_i$, $\eta_2=\cos\phi_t/\cos\phi_1$, $Q_{t0}=\partial\ln t_{0,1}^1(k_{\perp 0})/\partial k_{\perp 0}\big|_{k_{\perp 0x}}$ and $Q_{t1}=\partial\ln t_{1,2}^1(k_{\perp 1})/\partial k_{\perp 1}\big|_{k_{\perp 1x}}$.

After inserting the amplitude transmittance expressions (19) and (20) into the integral (9), the total transmitted electric field component can be written in the following form:

$$
\begin{aligned}
&E_t\left(r_t,\theta_t,z_t\right)=\frac{2^{-|l|}w_0^{|l|+2}k_t}{n_t}\sum_{k=0}^{|l|}b_k^{|l|}\frac{s_l^k}{i^{|l|-k+1}}\left(\frac{Z_{t1}}{1+Z_{t1}}\right)^{(|l|-k)/2}\exp\left(\frac{X_t^2}{1+Z_{t1}}\right)\left(\frac{Z_{t2}}{1+Z_{t2}}\right)^{k/2}H_k\left(\frac{Y_t}{\sqrt{Z_{t2}-Z_{t2}^2}}\right)\exp\left(\frac{Y_t^2}{1+Z_{t2}}\right)\cdot\\
&\left[t'H_{|l|-k}\left(\frac{X_t}{\sqrt{Z_{t1}-Z_{t1}^2}}\right)+t''\frac{2X_t}{w_0Z_{t1}}H_{|l|-k}\left(\frac{X_t}{\sqrt{Z_{t1}-Z_{t1}^2}}\right)-\frac{t''}{w_0\sqrt{Z_{t1}-Z_{t1}^2}}H_{|l|-k+1}\left(\frac{X_t}{\sqrt{Z_{t1}-Z_{t1}^2}}\right)\right]
\end{aligned}
\tag{21}
$$

where $b_k^{|l|}=\sqrt{\frac{(N-k)!k!}{2^Np!(\mathrm{p}+|l|)!}}\frac{1}{k!}\frac{d^k}{d\xi^k}\left[\left(1-\xi\right)^p\left(1+\xi\right)^{p+|l|}\right]\Big|_{\xi=0}$, $N=2p+|l|$, $X_t=ix_t/\eta_2w$, $Y_t=iy_t/w_0$, $Z_{t1}=iz_t/z_{Rx}$, $Z_{t2}=iz_t/z_{Ry}$, $z_{Rx}=\eta_2^{\,2}z_{R2}$, $z_{Ry}=z_{R2}$, $z_{R2}=k_tw_0^2/2$, $s_l=\mathrm{sgn}(l)$, and $H_n(x)$ is the Hermite polynomial. In the process of solving the integral (9), the relationship between the transformation relation between LG modes and HG modes [25] was used. It should be noticed that in order to derive the approximate

analytical expressions of equations(17) and (21), we consider only the prompt reflection and transmission, plus the first delayed reflection and transmission rather than the entire infinite series of them.

3. Numerical results and discussion

According to the expressions for the reflected and transmitted fields presented above, the characteristics of an LG beam incident on a dielectric slab are simulated and discussed in this section. In the simulation, the wavelength of incident beam is $0.6328\mu m$ (which is the wavelength of a He-Ne laser), the thickness of the slab is 500λ, and the distance from the beam waist center to the position of detector is $10cm$.

Effects of beam-waist radius:

The intensity distribution of reflected wave is shown in Figure2, which includes 8 panels. The panels (a1), (a2), (a3) and (a4) are reflected intensities from the first interface of the slab, and panels (b1), (b2), (b3) and (b4) are the total reflected intensities from the two interfaces of the slab. The radial index and topological charge of the incident beam are $p=0$ and $l=1$, respectively. The refractive indices for the input region and output region are 1.57 and 1.198, respectively. For the first three rows, the refractive index of the slab is1.20. To observe the effects of the lossy media, we assume that the refractive index of the slab in the last row is $1.2+i0.01$. The incident angle is chosen to be 49.7 degrees, which is very close to the critical angle.

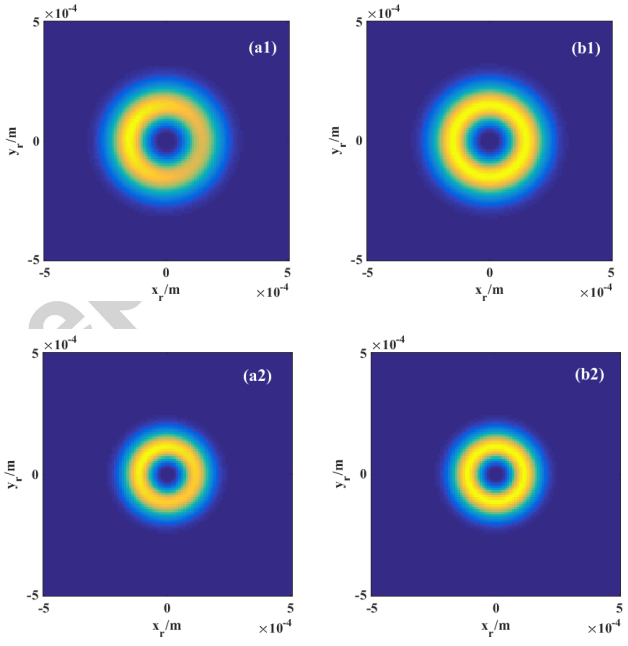

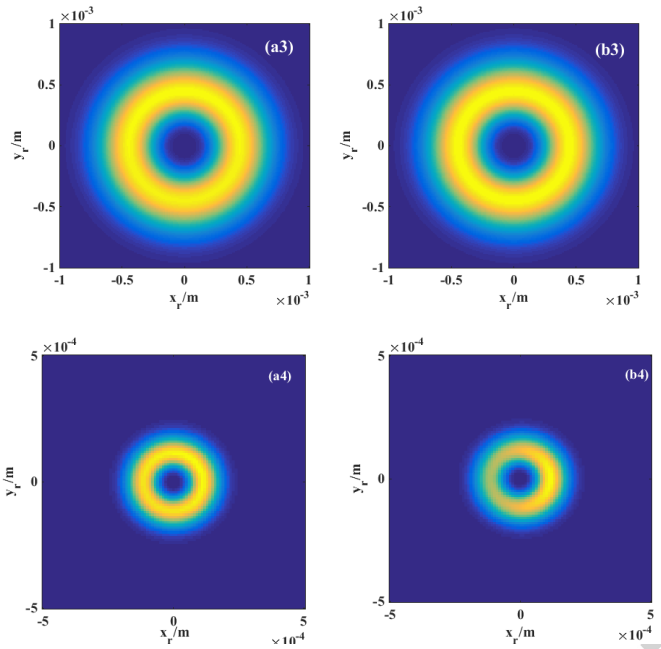

Figure2 Intensity distribution of the reflected beam. The first three rows are the results for a lossless slab, and the last row is the simulation for a lossy slab. The beam-waist radius of incident beams for (a1, b1), (a2, b2), (a3, b3) and (a4, b4) are 100λ , 200λ , 1000λ *and* 200λ *, respectively.*

Figure2 obviously shows that the reflected intensity still roughly maintains its circular shape, which is similar to the incident LG beam. This result is consistent with the conclusion in reference [26]. Compared with the reflected intensity of the first interface, the distortion of the total reflected intensity is not apparent, because of the multiple reflections between the first and the second interface and the refraction of the first interface. A comparison of the first three rows leads to the conclusion that as the beam-waist radius increases, the contour size of intensity decreases firstly and increases afterwards, and the distortion of reflected beam becomes gradually weak. Compared the last row with the second row, the total intensity distortion is found to be more evident in the case of a lossy medium.

With the same beam and media parameters, using the formula in equation (21), the intensity distribution of transmitted beam in the local coordinate (x_t, y_t, z_t) is presented in Figure 3. The panels (a1), (a2), (a3) and (a4) represent the transmitted intensities from the first interface of the slab, and panels (b1), (b2), (b3) and (b4) illustrate the total transmitted intensities from the two interfaces of the slab.

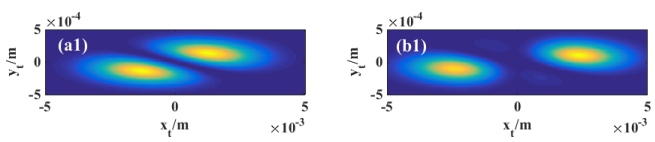

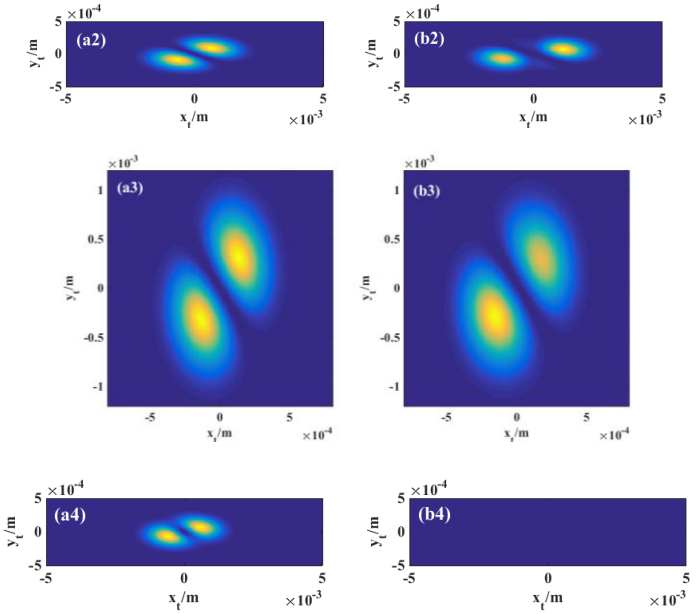

Figure3 Intensity distribution of the transmitted beam. The first three rows are simulations for a lossless slab, and the last row presents the results for a lossy slab. The beam-waist radius of incident beams for (a1, b1), (a2, b2), (a3, b3) and (a4, b4) are 100λ , 200λ , 1000λ *and* 200λ *, respectively.*

The shape of transmitted beam is no longer circular, and is somewhat similar to the diagonal Hermite beam mode. In the first and second row, compared with the distribution along the y_t axis, the intensity distribution is broadened greatly in the direction of the x_t axis. However, when the beam-waist radius reaches 1000λ , the broadening is more evident along the y_t axis. As the beam-waist radius increases, broadening along the x_t axis direction becomes less apparent whereas in the y_t axis direction it becomes larger. The regularity of contour size variation of transmitted intensity is similar to the case of reflected intensity. Compared the transmitted intensity of the first interface with the total transmitted intensity, we can find that the two parts of the intensity contour for the first interface have almost a symmetrical distribution, but the contour of the total intensity is no longer symmetrical as follows: as the beam-waist radius increases, the left part of the total intensity decreases gradually. When the refractive index of slab is $1.2+i0.01$, a comparison of the results in the second row with that of the last row shows that, because of the absorption, the total transmitted intensity becomes zero, and the intensity contour size of the first interface is also smaller.

Effects of topological charge:

For the purpose of discussing the effects of topological charge *l* on the reflected and transmitted intensity distribution, the intensity distribution with different topological charge *l* is shown in Figure 4. The beam-waist radius is kept at 1000λ . A comparison of Figure 4 (a1) with Figure 4 (a2) suggests that an increase on topological charge *l* enlarges the diameter of the reflected intensity ring, but does not change its shape; this phenomenon is similar to the effects on the incident LG beam. For the same beam-waist radius, compared with Figure3 (b3), the transmitted intensity of $p=1$, $l=1$ still has the very similar shape, whereas for the $p=1, l=2$ case, the

division between the two independent parts of transmitted intensity disappears.

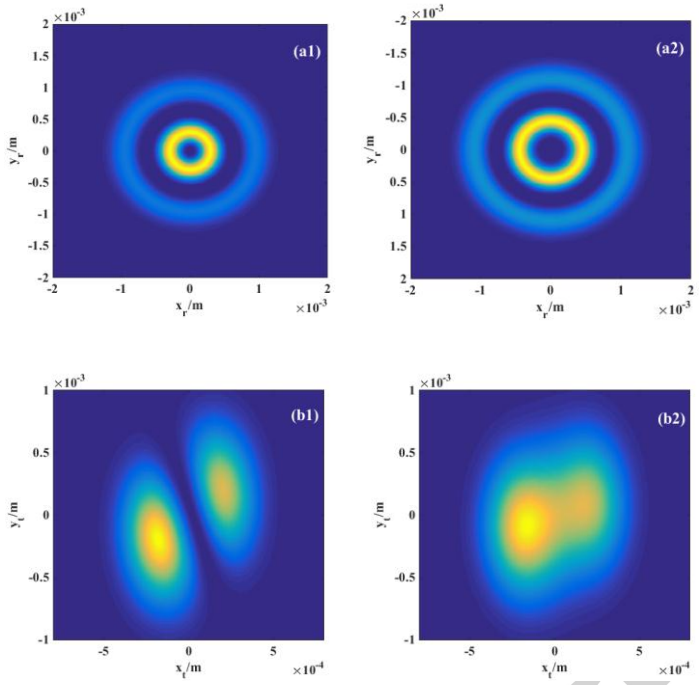

Figure4 Variations of topological charge on intensity distribution, (a1) reflected intensity: $p=1, l=1$ *; (a2) reflected intensity:* $p=1, l=2$ *; (b1)transmitted intensity:* $p=1, l=1$ *; (b2) transmitted intensity:* $p=1, l=2$ *.*

Centroid shifts of the reflected beam from a slab

When a beam is incident on the interface, the centroid of reflected and transmitted beams will shift in both transverse and longitudinal directions [21-23]. It is worth noticing that the intensity shifts in the direction of x_r axis and y_r axis in Figure 2 cannot be seen directly due to it is very small. Reference [26] provides a detailed discussion on the transverse and longitudinal shifts of reflected beam from one interface. To analyze the effects of the slab on the shift of reflected beam, the shift formulas must be derived. The centroid of a beam [39] can be determined by

$$\langle x_\alpha \rangle \hat{i}_\alpha + \langle y_\alpha \rangle \hat{j}_\alpha = \frac{\iint \left(x_\alpha \hat{i}_\alpha + y_\alpha \hat{j}_\alpha \right) I\left(x_\alpha, y_\alpha, z_\alpha\right) dx_\alpha dy_\alpha}{\iint I\left(x_\alpha, y_\alpha, z_\alpha\right) dx_\alpha dy_\alpha} \tag{22}$$

where $\hat{i}_\alpha$ and $\hat{j}_\alpha$ represent the unit vectors that point to the positive directions of x_α and y_α axes, respectively.

Considering the beam intensity is proportional to $|E|^2$, substituting the expression (17) into equation (22), the centroid shifts of the reflected beam from a dielectric slab are obtained as follows:

$$\langle x_r \rangle = \frac{w^2(z_r)\left\{\left(-\frac{{w_0}^2 k_0 z_r}{2 z_R}\right)\left(A_{10}A_{11}+A_{12}A_{13}\right)(2p+|l|+1)+A_{10}A_{12}(3p+3|l|+2)+A_{13}A_{14}(p+|l|)\right\}}{I_{total}} \tag{23}$$

$$\langle y_r \rangle = \frac{w^2(z_r)(A_{10}A_{11} + A_{12}A_{13})l}{I_{total}} \tag{24}$$

where $B_{100} = r_{12}^1(k_{\perp 1x})\left[Q_{1r}\cos\theta_1/\cos\theta_0 - 2\left(r_{01}^1(k_{\perp 0x})\right)^2 Q_{0r}\right]$,

$C_{100} = r_{12}^1(k_{\perp 1x})\left[1-\left(r_{01}^1(k_{\perp 0x})\right)^2 - k_{\perp 1x}Q_{r1} + 2k_{\perp 0x}\left[r_{0,1}^1(k_{\perp 0x})\right]^2 Q_{r0}\right]\exp(i2k_{1z}d_1)$,

$A_{10} = \left[r_{01}^1(k_{\perp 0x})(1-k_{\perp 0x}Q_{0r}) + C_{100}\cos(2k_1\cos\theta_1 d_1)\right]$, $A_{11} = \left[r_{01}^1(k_{\perp 0x})Q_{0r} + B_{100}\sin(2k_1\cos\theta_1 d_1)\right]$,

$A_{12} = B_{100}\sin(2k_1\cos\theta_1 d_1)$, $A_{13} = C_{100}\sin(2k_1\cos\theta_1 d_1)$, $A_{14} = \left[r_{01}^1(k_{\perp 0x})Q_{0r} + B_{100}\cos(2k_1\cos\theta_1 d_1)\right]$. The denominator in equations (23) and (24) is

$$\begin{aligned} I_{total} = {} & \left[(A_{10})^2 + (A_{13})^2\right]\frac{\pi w^2(z_r)}{2}\frac{(p+|l|)!}{p!} + \left[(A_{11})^2 + 2(A_{12})^2 + (A_{14})^2\right]\frac{p!|l|^2}{(p+|l|)!}\sum_{i=0}^{p}\frac{(i+|l|-1)!}{i!} + \\ & \left[\left[(A_{11})^2 + (A_{12})^2\right]\frac{{w_0}^4 {k_0}^2 {z_r}^2}{4{z_R}^2} + (A_{12})^2 + (A_{14})^2\right](2p+|l|+1) + \\ & \left[4\left({A_{12}}^2 + {A_{14}}^2\right) - A_{12}(A_{11}-A_{14})\frac{{w_0}^2 k_0 z_r}{z_R}\right](p+|l|+1) + \left[(A_{12})^2 + (A_{14})^2\right]2|l| - \\ & A_{12}(A_{11}+A_{14})\frac{{w_0}^2 k_0 z_r}{z_R}(|l|+2p+l+1) + 2\left({A_{12}}^2 - {A_{14}}^2\right)(p+2|l|+1) \end{aligned} \tag{25}$$

With the equations (23)-(25), variations of the centroid shifts of the reflected beam from a slab with incident angles are calculated and presented in Figure5. Using the expression in reference [40], the results of a single interface are drawn in blue in the same figure. Because of the effects of multiple reflections between two interfaces, the shift in the x_r axis is smaller than the result of the single interface case, whereas in the y_r axis they are very close. The effects of beam-waist radius on the shift in the x_r axis are more apparent than the effects on the shift in the y_r axis. In the y_r axis, the shift of the $w_0 = 100\lambda$ case almost coincides with that of the $w_0 = 200\lambda$ case.

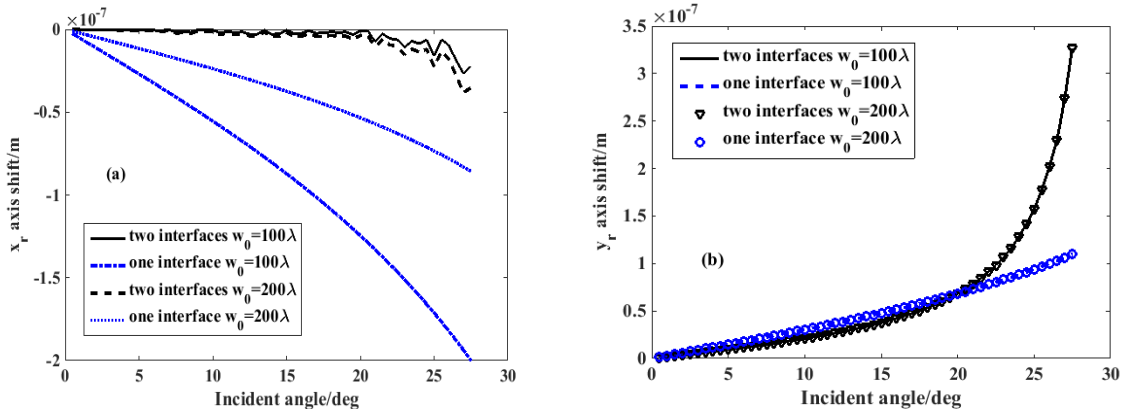

Figure5 Variations of the centroid shifts of the reflected beam in the direction of the (a) x_r and (b) y_r axis

After substituting equation (21) into equation (22), the centroid shifts of the transmitted field can be obtained. The similar conclusion applies to the transmitted field case.

4. Conclusion

Based on the plane-wave angular spectrum representation and the generalized Fresnel amplitude reflectance and transmittance, the reflected and transmitted fields of an LG beam incident on a dielectric slab were presented. With the Taylor series expansion, the approximate analytical formulas of reflected and transmitted fields were derived. When the incident beams had different beam-waist radii and different topological charges, the distributions of reflected and transmitted intensities were simulated. The results for a lossy slab were also presented. It was concluded that the distortion of intensity distribution including the size of intensity contour was greatly influenced by the beam-waist radii and the topological charges. The effects of beam-waist radius on reflected intensity of a single interface were found to be more evident. The total transmitted intensity of two interfaces was distinguishable from the case of a single interface. The total reflected and transmitted intensities for a lossy slab are obviously distorted. An increase on topological charge l was found to increase the diameter of the reflected intensity ring, but did not change its shape, while greatly changing the distribution of transmitted intensity. The centroid shifts of reflected intensity can be obtained in our simulation. Expressions of the centroid shifts of reflected beams were presented, and the variation of shifts with incident angles was calculated and compared with the results of one interface. Although the beam-waist radius of incident beam had significant effects on the intensity distribution and shifts in the x_r axis, its effects on the centroid shifts of reflected beams in the y_r axis were not very obvious. With the help of transmitted field expression, similar predictions of the centroid shifts of transmitted beam can also be obtained.

The derived formulas mentioned above can be applied to analyzing the propagation characteristics of LG beams with different topological charges l in isotropic inhomogeneous media, which is an important part of vortex beam communication.

5. Acknowledgement

This work is supported by the National Natural Science Foundation of China under grants 61475123, 61571355, 61308025, overseas training program for young backbones teachers sponsored by China Scholarship Council (CSC) and Xidian University, and the Project Supported by Natural Science Basic Research Plan in Shaanxi Province of China under grant 2016JQ4015.

6. References

[1] L. Allen, M. W. Beijersbergen, R. J.C. Spreeuw, and J. P. Woerdman, "Orbital angular momentum of light and the transformation of Laguerre–Gaussian laser modes," Phys. Rev. A 45, 8185-8189,1992.

[2] E. Karimi, B. Piccirillo, E. Nagali, L. Marrucci, and E. Santamato, "Efficient generation and sorting of orbital angular momentum eigenmodes of light by thermally tuned q-plates," APPLIED PHYSICS LETTERS, vol. 94, 231124, 2009.

[3] E. Karimi, S. A. Schulz, I. De Leon, H. Qassim, J. Upham, and R. W. Boyd, "Generating optical orbital angular momentum at visible wavelengths using a plasmonic metasurface," Light: Science and Applications, vol. 3, e167, 2014.

[4] W. B. Wang, R. Gozali, L. Shi, L. Lindwasser and R. R. Alfano, "Deep transmission of Laguerre–Gaussian vortex beams through turbid scattering media," Optics Letters, vol. 41, 2069-2072, 2016.

[5] V. P. Aksenov and C. E. Pogutsa, "Fluctuations of the orbital angular momentum of a laser beam, carrying an optical vortex, in the turbulent atmosphere," Quantum Electronics, vol. 38, 343-349, 2008.

[6] M. E. J. Friese, J. Enger, H. Rubinsztein-Dunlop, N. Heckenberg, "Optical angular-momentum transfer to trapped absorbing particles," Phys. Rev. A vol. 54, 1593-1596. 1996.

[7] Eleonora Nagali, Fabio Sciarrino, Francesco De Martini, Lorenzo Marrucci, Bruno Piccirillo, Ebrahim Karimi, and Enrico Santamato, "Quantum Information Transfer from Spin to Orbital Angular Momentum of Photons," Phys. Rev. Lett. vol.103, 013601, 2009.

[8] M. Malik, "Influence of atmospheric turbulence on optical communications using orbital angular momentum for encoding," Opt. Express, vol.20, 13195, 2012.

[9] G. Foo, D. M. Palacios, Jr.G.A. Swartzlander, "Optical vortex corona graph," Opt. Lett., vol. 30, 3308–3310, 2005.

[10] N. s. Uribe-Patarroyo, A. Fraine, D. S. Simon, O. Minaeva, and A. V. Sergienko, "Object Identification Using Correlated Orbital Angular Momentum States," PHYSICAL REVIEW LETTERS, vol. 110, 043601, 2013.

[11] J. A. Fleck and M. D. Feit, "Beam propagation in uniaxial anisotropic media," J. Opt. Soc. Am., vol. 73, 920-926, 1983.

[12] H. Schmidt and F. B. Jensen, "A full wave solution for propagation in multilayered viscoelastic media with application to Gaussian beam reflection at fluid–solid interfaces," The Journal of the Acoustical Society of America, vol. 77, pp. 813-825, 1985.

[13] G. Gouesbet, B. Maheu, and G. Gréhan, "Light scattering from a sphere arbitrarily located in a Gaussian beam, using a Bromwich formulation," J. Opt. Soc. Am. A, vol. 5, 1427-1443, 1988.

[14]Michael I. Mishchenko, Joachim W. Hovenier, Larry D. Travis, "Light Scattering by Nonspherical Particles: Theory, Measurements, and Applications"，Academic Press, 1999.

[15] Piero Bruscaglioni, Giovanni Zaccanti, and Qingnong Wei, "Transmission of a pulsed polarized light beam through thick turbid media: numerical results," Appl. Opt., vol.32, 6142-6150, 1993.

[16] G. Gouesbet and G. Grehan, "Generalized Lorenz-Mie Theories, From Past to Future," vol. 10, 277-333, 2000.

[17] Changjun Min, Pei Wang, Xiaojin Jiao, Yan Deng, and Hai Ming, "Beam manipulating by metallic nano-optic lens containing nonlinear media," Opt. Express, vol.15, 9541-9546, 2007.

[18] U. Vyas and D. Christensen, "Ultrasound Beam Simulations in Inhomogeneous Tissue Geometries Using the Hybrid Angular Spectrum Method," IEEE Transactions on Ultrasonics, Ferroelectrics, and Frequency Control, vol. 59, 1093-1100, 2012.

[19] Y. ANTAR and W. M. BOERNER, "Gaussian Beam Interaction with a Planar Dielectric Interface," CAN. J . PHYS., vol. 52, 962-972, 1974.

[20] C. Chiu Chan and T. Tamir, "Angular shift of a Gaussian beam reflected near the Brewster angle," Opt. Lett., Vol.10, 378-380, 1985.

[21] Y. Wang, Y. Liu, J. Xu, H. Zhang, L. Bai, Y. Xiao, et al., "Numerical study of lateral displacements of Gaussian beams reflected from weakly absorbing media near the Brewster dip and reflected from strongly absorbing media," J. Opt. A: Pure Appl. Opt., vol. 11, 105701, 2009.

[22] K. Y. Bliokh, I. V. Shadrivov, and Y. S. Kivshar, "Goos–Hänchen and Imbert–Fedorov shifts of polarized vortex beams," Opt. Lett., vol. 34, 389-391, 2009.

[23] K. Y. Bliokh and A. Aiello, "Goos–Hänchen and Imbert–Fedorov beam shifts: an overview," J. Opt., vol. 15, 014001, 2013.

[24] N. I. Petrov, "Reflection and transmission of strongly focused vector beams at a dielectric interface," Opt. Lett., vol. 29, 421-423, 2004.

[25] H. Okuda and H. Sasada, "Significant deformations and propagation variations of Laguerre–Gaussian beams reflected and transmitted at a dielectric interface," J. Opt. Soc. Am. A, vol. 25, 881-890, 2008.

[26] J. Ou, Y. Jiang, J. Zhang, and Y. He, "Reflection of Laguerre–Gaussian beams carrying orbital angular momentum: a full Taylor expanded solution," J. Opt. Soc. Am. A, vol. 20, 2561-2570, 2013.

[27] R. P. Riesz and R. Simon, "Reflection of a Gaussian beam from a dielectric slab," J. Opt. Soc. Am. A, vol.2, 1809-1817, 1985.

[28] Richard W. Ziolkowski, "Pulsed and CW Gaussian beam interactions with double negative metamaterial slabs," Opt. Express, vol. 11, 662-681, 2003.

[29] M. J. Wang, H.Y. Zhang, G.S. Liu, Y.L. Li, and Q.F. Dong, "Reflection and transmission of Gaussian beam by a uniaxial anisotropic slab," Opt. Express, vol. 22, 3705-3711, 2014.

[30]J. A. Kong, B.-I. Wu, and Y. Zhang, "A unique lateral displacement of a Gaussian beam transmitted through a slab with negative permittivity and permeability," Microwave and Optical Technology Letters, vol. 33, pp. 136-139, 2002.

[31] P.G. Galiatsatos and V. Yannopapas, "Optical manipulation of a particle placed within a planar dielectric cavity," Journal of Modern Optics, vol. 56, 744-750, 2009.

[32] H. Mao, T. Zang, J. Sun, T. Pan, and G. Xu, "Goos–Hänchen shifts of the reflected waves from the inhomogeneous slab with a positive and negative index transition layer," Phys. Status Solidi B, vol. 249, 829-833, 2012.

[33] F. Falco and T. Tamir, "Improved analysis of nonspecular phenomena in beams reflected from stratified media," J. Opt. Soc. Am. A, vol. 7, 185-190, 1990.

[34] V. Shah and T. Tamir, "Absorption and lateral shift of beams incident upon lossy multilayered media," J. Opt. Soc. Am., vol. 73, 37-44, 1983.

[35] U. Vyas and D. Christensen, "Ultrasound Beam Simulations in Inhomogeneous Tissue Geometries Using the Hybrid Angular Spectrum Method," IEEE Transactions on Ultrasonics, Ferroelectrics, and Frequency Control, vol. 59, 1093-1100, 2012.

[36] L. W. Casperson, "Gaussian Light Beams in Inhomogeneous Media," Appl. Opt., vol. 12, 2434-2441, 1973.

[37] M. Lax, W. H. Louisell, and W. B. McKnight, "From Maxwell to paraxial wave optics," Phys. Rev. A, vol.11, 1365–1370, 1975.

[38] W. C. Chew, Waves and Fields in Inhomogeneous media. New York: IEEE Antennas and Propagation Society, Sponsor, 1995.

[39] A. Aiello and J. P. Woerdman, "Role of beam propagation in Goos- Hänchen and Imbert-Fedorov shifts," Opt. Lett., vol. 33, 1437-1439, 2008.

[40] J. Ou, Y. Jiang, F. Li, L. Liu, "Shifts of beam centroid of Laguerre-Gaussian beams reflected and refracted at a dielectric interface," Acta Phys. Sin., vol. 60, 114203, 2011.

Highlights

- Reflection and transmission of LG beam incident on a dielectric slab are described on the basis of plane-wave angular spectrum representation.
- Analytical expressions of total reflected and transmitted fields of a dielectric slab are derived.
- Effects of beam-waist radius and topological charge on reflected and transmitted field intensities are simulated.
- Centroid shifts of reflected beam of a dielectric slab are presented and discussed.